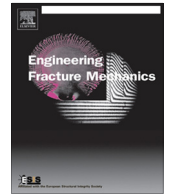




ELSEVIER

Contents lists available at ScienceDirect

Engineering Fracture Mechanics

journal homepage: www.elsevier.com/locate/engfracmech

A non-local approach to crack process modeling in ceramic materials subjected to thermal shock

Jia Li^{a,*}, Fan Song^b, Chiping Jiang^c^a LSPM, CNRS UPR 3407, Université Paris XIII, Villetaneuse, France^b State Key Laboratory of Nonlinear Mechanics, Institute of Mechanics, Chinese Academy of Sciences, Beijing, China^c Solid Mechanics Research Center, Beijing University of Aeronautics and Astronautics, Beijing, China

ARTICLE INFO

Article history:

Received 18 April 2014

Received in revised form 2 November 2014

Accepted 17 November 2014

Available online 22 November 2014

Keywords:

Non-local model

Multiple cracking

Thermal shock

Finite element analysis

Ceramics

ABSTRACT

In this paper, we present a non-local approach to fracture modeling in brittle or quasi-brittle materials and its finite element implementation. The proposed fracture model is constructed on the basis of the conventional maximal principal stress criterion for uniform tensile loads and the Griffith–Irwin criterion for crack propagation prediction. Consequently, the proposed fracture criterion can be used to predict both the crack initiation and the crack growth. Moreover, we also showed that when the element size is much smaller than the characteristic length scale of the material, the proposed fracture model is mesh-independent. By using the proposed model, we carried out detailed numerical simulations on cracking process of ceramic materials subjected to thermal shock loading. The comparison with the experimental results shows that the periodic and hierarchical structure of the crack pattern is faithfully reproduced by the numerical simulations.

© 2014 Elsevier Ltd. All rights reserved.

1. Introduction

Fracture assessment in brittle or quasi-brittle materials is an essential but difficult task in computational mechanics. Developing efficient and accurate finite element models to simulate tensile fracture behavior has been extensively studied in the last two decades. Two types of fracture models, i.e., the damage-mechanics-based models and fracture-mechanics-based models, are most frequently used in cracking simulations. The damage-mechanics-based models assume that the fracture is caused by continuously varying damage in the solid. The crack propagation is described by reducing the material stiffness and strength of the elements. The fracture-mechanics-based models are based on displacement discontinuity between crack surfaces, usually represented by nonlinear interface elements. The constitutive behavior of such elements is described by softening relations between traction and crack relative displacements, as assumed by the cohesive crack model.

The damage-mechanics-based models have been very popular because of its computational convenience [1–6]. These models present numerous advantages such as their capacity in dealing with default development before formation of macro-cracks, the possibility to include micromechanics-based behaviors and the easy numerical implementation. One drawback of the damage-mechanics-based models may be the large spread damage zones, which can hardly be regarded as cracks. On the other hand, the fracture-mechanics-based models have also been largely investigated. Enormous success

* Corresponding author at: LSPM, CNRS UPR 3407, Institut Galilée, Université Paris 13, 99 Avenue Jean-Baptiste Clément, 93430 Villetaneuse, France. Tel.: +33 1 49 40 28 89; fax: +33 1 49 40 39 38.

E-mail address: jia.li@univ-paris13.fr (J. Li).

Nomenclature

σ_1	first principal stress
σ_c	ultimate tensile stress
$\bar{\sigma}_{ij}$	non-local stress
$\bar{\sigma}_1$	non-local first principal stress
$\delta\Pi$	variation of potential energy
δE	variation of kinetic energy
δl	crack growth vector
\bar{p}	dimensionless crack length
\bar{s}	dimensionless crack spacing
δS	newly created crack surface
ν	Poisson's ratio
α	thermal expansion coefficient
ρ	mass density
φ, ψ	space weighting functions
c	specific heat
D	damage
d	side length of the triangle elements.
E	Young's modulus
G_c	fracture energy per unit surface
h	convective heat transfer coefficient
k	thermal conductivity
K_I	stress intensity factor
K_{Ic}	critical stress intensity factor
R	radius of the non-local interaction area
r_0	distance between the crack tip and the position where the non-local tensile stress is maximal
T	temperature field in quenched specimens
T_0	initial temperature of specimens
T_∞	water temperature in quenching bath

has been achieved in fracture analysis with the cohesive model [7–11] or the extended-finite element method (XFEM) [12–16]. The main advantages of these crack models remain in their strictness in analysis; the accurate solutions and easily applied criteria.

Simulating multi-cracking phenomenon is a formidable challenge for numerical fracture mechanics. The ability to predict both the crack initiation and crack growth, the mesh-independency of the numerical results, the stable, robust, accurate and low-cost numerical algorithms are some essential exigencies for fracture models simulating such a phenomenon. Francfort and Marigo [17] developed a so-called damage gradient model in which the damage zone converges to a crack as the length parameter tends to zero. Efficient algorithms were developed in order to resolve complicated cracking problems [18,19]. Pijaudier-Cabot and Bazant [20,21] developed a practical nonlocal model in a continuum damage setting. The development of nonlinear gradient models, initially developed in plasticity behavior description, has afterwards been transferred to damage mechanics [22,23]. Another method involves lattice simulation that considers a solid as a network of bars or beams [24–26]. Several attempts by modeling directly micro-cracks and their growth were reported in earlier researches by using the boundary element method [27–29].

In the framework of notch fracture analysis, the so-called finite fracture mechanics was developed. Neuber [30] first proposed the effective stress criterion based on average stress over a characteristic length related to the notch radius. The failure criterion, proposed by Novozhilov [31] and expanded by Seweryn [32], suggests considering the mean normal stress along the anticipated path of the failure. Pluvinage [33] proposed averaging the stress distribution over the entire process volume to establish more accurate fracture criteria. Introduction of a length scale parameter in crack growth criteria was successively used to predict the crack initiation or to take the non-linear mechanisms into account for crack growth [34–39]. The principal advantage of this class of theories resides in their accuracy and simplicity. However, these analyses were suitable only for individual crack formation and evolution. On the basis of the finite fracture mechanics concept, Li et al. [40,41] developed a Fast Fourier Transform (FFT) code, which is capable to simulate multiple crack onset and crack growth in brittle materials.

In this paper, the ideas described in Li et al. [40,41] were essentially followed. However, the FFT modeling is appropriate only for analyses of periodic structures under periodic loading; Moreover, the criterion proposed in Li et al. [40,41] is capable to forecast the position, but not the orientation and length of the new crack. In the present work, this model is improved and implemented to a finite element code. Thus the location, orientation and length of the newly created crack are explicitly determined. We have demonstrated that the proposed fracture criterion can be used to predict both the crack initiation and the crack growth. Moreover, its mesh-independency was also discussed through some numerical examples.

Using the established non-local damage model, we carried out detailed numerical simulations on cracking process of the ceramic specimens under thermal shock loading. The crack pattern formation under thermal shock is a very rapid and highly complex process. In fact, the multi-cracking phenomenon such as that observed in thermal shock experiments is intrinsically difficult to simulate. The proposed model in the present work allows a highly realistic cracking simulation. Comparison with the experiments shows that the multi-cracking process was faithfully reproduced by numerical simulations. The predicted crack paths and the characteristics of the crack patterns agree excellently with the experimental observation.

2. A non-local fracture criterion

In this section, we describe the establishment of the non-local fracture model for brittle and quasi-brittle materials.

2.1. Crack onset and crack growth criterion

The commonly used maximum stress fracture criterion for brittle material is the start point in constructing the non-local fracture criterion, namely:

$$D = \begin{cases} 0 & \sigma_1 < \sigma_c \\ 1 & \sigma_1 \geq \sigma_c \end{cases} \quad (1)$$

where D is the damage of the considered element; σ_1 is the first principal stress and σ_c is the ultimate tensile stress of the material. According to this criterion, the element will be instantaneously broken when the first principal stress reaches the material strength.

If this strength criterion is acceptable to predict the failure of a non-cracked structure, however, it is not suitable to predict fractures due to crack. In order to overcome this shortcoming, various methods have been proposed. Among these methods, the so-called non-local approach [20] is widely used. The non-local stress field can be calculated as follows:

$$\tilde{\sigma}_{ij} = \int_V \varphi(\mathbf{x} - \mathbf{y}) \sigma_{ij}(\mathbf{y}) d\mathbf{y} \quad (2)$$

where $\varphi(\mathbf{x} - \mathbf{y})$ is a space weighting function which describes the mutual non-local interactions and depends only on the distance between the source point \mathbf{x} and the receiver point \mathbf{y} . Mathematically, the normalization condition $\int_V \varphi(\mathbf{x} - \mathbf{y}) d\mathbf{y} = 1$ is required. Hereafter we adopt the following weighting function:

$$\varphi(\mathbf{x} - \mathbf{y}) = \frac{\psi(\mathbf{x} - \mathbf{y})}{\int_V \psi(\mathbf{y}) d\mathbf{y}} \quad (3)$$

Therefore, the non-local first principal stress in a 2D structure writes:

$$\tilde{\sigma}_1(\mathbf{x}) = \frac{\tilde{\sigma}_{11} + \tilde{\sigma}_{22}}{2} + \sqrt{\left(\frac{\tilde{\sigma}_{11} - \tilde{\sigma}_{22}}{2}\right)^2 + \tilde{\sigma}_{12}^2} \quad (4)$$

By means of this non-local principal stress, the damage model (1) can be rewritten as follows:

$$D = \begin{cases} 0 & \tilde{\sigma}_1 < \sigma_c \\ 1 & \tilde{\sigma}_1 \geq \sigma_c \end{cases} \quad (5)$$

It is clear that the main tasks in the construction of this non-local fracture criterion are how to determine the weighting function $\alpha(\mathbf{x} - \mathbf{y})$ and the non-local interaction volume V . In 2D calculations and for simplicity, we define V as a circle of radius R and centered at the source point \mathbf{x} . For simplicity, a cone-shaped function is chosen as the weighting function ψ :

$$\psi(r) = \begin{cases} 0 & r > R \\ 1 - \frac{r}{R} & r \leq R \end{cases} \quad (6)$$

where $r = \|\mathbf{x} - \mathbf{y}\|$ is the distance between the points \mathbf{x} and \mathbf{y} . Therefore, the single parameter to determine is R , the radius of the non-local interaction area. To this end, we enforce the criterion (5) to be exact in two special stress states as follows:

1. It must be exact for fracture prediction under uniform tensile loading.

In this case, the non-local stress field is exactly equal to the local stress field. Therefore, the non-local fracture criterion (5) is exactly equivalent to the local fracture criterion (1).

2. It must be exact for propagation prediction of a mode-I crack.

In this case, the crack grows if the Griffith–Irwin criterion $K_I \geq K_{Ic}$ is satisfied, where K_I is the stress intensity factor of the crack tip and K_{Ic} is its critical value [42,43]. We first prove that the non-local fracture criterion (5) can be connected to the Griffith–Irwin criterion. Consider a mode-I loaded macro-crack. According to the Williams asymptotic solution [44], the stresses at a point near the crack tip are modulated by the stress intensity factor K_I as follows:

$$\begin{aligned}
 \sigma_{11} &= \frac{K_I}{\sqrt{2\pi r}} f_{11}(\theta) & f_{11} &= \cos \frac{\theta}{2} \left(1 - \sin \frac{\theta}{2} \sin \frac{3\theta}{2} \right) \\
 \sigma_{22} &= \frac{K_I}{\sqrt{2\pi r}} f_{22}(\theta) & f_{22} &= \cos \frac{\theta}{2} \left(1 + \sin \frac{\theta}{2} \sin \frac{3\theta}{2} \right) \\
 \sigma_{12} &= \frac{K_I}{\sqrt{2\pi r}} f_{12}(\theta) & f_{12} &= \cos \frac{\theta}{2} \sin \frac{\theta}{2} \cos \frac{3\theta}{2}
 \end{aligned}
 \tag{7}$$

where r and θ are the polar coordinates of this point. The non-local principal stresses at a near-tip point (r_0, θ_0) write:

$$\tilde{\sigma}_{ij}(r_0, \theta_0) = K_I \int_{-\pi}^{\pi} \int_0^R \varphi(r', \theta') \frac{1}{\sqrt{2\pi r'}} f_{ij}(\theta) r' dr' d\theta'
 \tag{8}$$

According to (2), (4) and (8), the non-local first principal stress can be written as follows:

$$\tilde{\sigma}_1(r_0, \theta_0) = K_I \Sigma(R, r_0, \theta_0)
 \tag{9}$$

The function $\Sigma(R, r_0, \theta_0)$ can straightforwardly be obtained from (4), (7) and (8). The geometrical quantities in (10) and (11) are illustrated in Fig. 1. From Fig. 1, we have the following relationships between these quantities:

$$r \cos \theta = r_0 \cos \theta_0 + r' \cos \theta' \quad r \sin \theta = r_0 \sin \theta_0 + r' \sin \theta'$$

These relationships permit us to evaluate the non-local first principal stress field according to (8) and (9).

On one hand, if we assume that $\tilde{\sigma}_1(r_0, \theta_0)$ is the maximal value of the non-local principal stresses near the crack tip, this point will be broken when $\tilde{\sigma}_1(r_0, \theta_0) \geq \sigma_c$ according to the damage criterion (5). On the other hand, from the Griffith–Irwin criterion of fracture [42,43], the crack grows when the stress intensity factor K_I attains its critical value K_{Ic} . Thus we obtain the condition of the damage for this point:

$$\sigma_c = K_{Ic} \Sigma(R, r_0, \theta_0)
 \tag{10}$$

This condition permits to determine the geometrical parameters R , r_0 and θ_0 . For a mode-I crack growth, it is clear that $\theta_0 = 0$. The parameters R and r_0 can be evaluated by resolving numerically the following optimization problem:

$$F(R) = \sigma_c - K_{Ic} \max_{r_0} \Sigma(R, r_0) = 0
 \tag{11}$$

In fact, the parameters R and r_0 are material-dependent. Especially the non-local action radius R is proportional to $(K_{Ic}/\sigma_c)^2$.

This analysis leads us to establish the following non-local crack initiation and crack growth criterion: Find the point where the non-local first principal stress is maximal, a new crack perpendicular to the maximal non-local first principal stress will appear at this point if $\tilde{\sigma}_1 \geq \sigma_c$.

As the proposed non-local fracture criterion is exact for crack onset prediction under uniform tensile loading and for the propagation prediction of a mode-I crack, the fracture prediction under other types of stress concentrations can just be considered as a natural interpolation between the two former special cases. Consequently, the proposed fracture criterion can be applied to predict the crack onset as well as the crack growth with high accuracy.

Another feature of this criterion is that it does not need to handle the propagation of individual cracks in the solid. Consequently, multi-crack problems can easily be assessed without evaluate individually each crack toughness.

In Table 1, we list the indicative values of R and r_0 of some brittle materials estimated from (11) according to the above-described method. The values of K_{Ic} and σ_c are extracted from [45].

From this table, we can give a reasonably accurate estimation of the values of R and r_0 by using the following simple formulas:

$$\begin{aligned}
 R &= \frac{1.05}{\pi} \left(\frac{K_{Ic}}{\sigma_c} \right)^2 \\
 r_0 &= 0.4R
 \end{aligned}
 \tag{12}$$

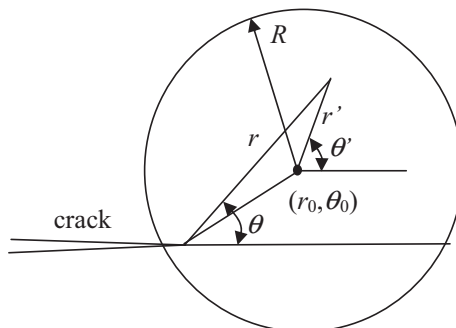


Fig. 1. Non-local action zone.

Table 1

Non-local parameters R and r_0 for some brittle materials.

	K_{Ic} (MPa $\sqrt{\text{mm}}$)	σ_c (MPa)	R (mm)	r_0 (mm)
Glass	22	80	0.0256	0.0102
Epoxy (PMMA)	36	72	0.0835	0.033
Alumina	94	220	0.0631	0.025
Graphite cast iron	1220	500	1.925	0.79
Concrete	12.65	4	3.334	1.325

2.2. Length of crack extension

The above-described fracture criterion predicts the apparition of a newly created crack. Under some special conditions, we can evaluate the length of the new crack.

We consider the initial state of a loaded structure to be elasto-static. Next, we consider the same structure after the onset of a new crack or the growth of a preexisting one. The energy balance between these two states writes:

$$\delta\Pi + \delta E + G_c \delta S = 0 \tag{13}$$

Here, $\delta\Pi$ and δE are the changes respectively in potential and kinetic energy. The newly created crack surface is denoted δS and G_c is the fracture energy per unit surface, the so-called toughness. In quasi-static analysis, we can assume that the initial and final states are static and then $\delta E = 0$. Eq. (13) permits us to evaluate the new fracture surface during the cracking process:

$$\delta S = -\frac{\delta\Pi}{G_c} \tag{14}$$

In general, (14) is a transcendent equation that is difficult to resolve. This is because that first, $\delta\Pi$ is function of δS and second, δS may depend on numerous parameters describing the shape of the newly cracked surface.

In 2D problems, the crack growth can be represented by means of a vector $\vec{\delta l}$ that is perpendicular to the first principal direction. The length of $\vec{\delta l}$ can be divided into two part, namely $|\vec{\delta l}| = r_0 + dl$, as shown in Fig. 2. Thus we can write:

$$dl = -\frac{\delta\Pi(dl)}{G_c} - r_0 \tag{15}$$

The solution of this transcendent equation by iteration gives us an estimation of $\vec{\delta l}$.

3. Finite element implementation

Since the material is considered as linearly elastic before its complete damage, the crack propagation evaluation is just a sequence of linear analyses on the cracked structure. The linear feature of the present approach permits us to avoid complicated non-linear analysis and therefore to construct stable and robust algorithms.

In the framework of the proposed criterion, the crack propagation can be realized by determining the crack growth vector $\vec{\delta l}$. To this end, we find first the point where the non-local first principal stress is maximal; then we create a new crack of length $\delta l = r_0 + dl$, with dl in the crack growing direction and r_0 in the opposite direction, see Fig. 2.

The simplest manner to create a crack along a line is to eliminate all elements in intersection with this line. Hereafter we give the algorithm used in the finite element implementation:

1. For a given loading step, resolve the linear elastic problem by using the finite element method. Set an initial value of dl .
2. Calculate the total potential energy, noticed Π_1 .
3. Calculate the non-local principal stress field; Find the point \mathbf{x}_d where the non-local principal stress is maximal. Determine the two possible crack growth directions, as shown in Fig. 3a.
4. If $\tilde{\sigma}_1 \leq \sigma_c$, go to step 1.
5. Otherwise compare the average non-local first principal stresses along the two directions in order to determine the crack growth direction.

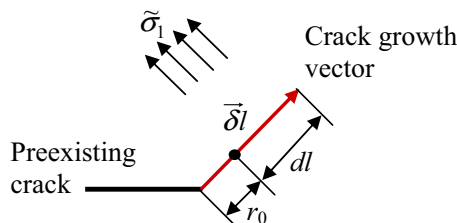


Fig. 2. Crack growth vector.

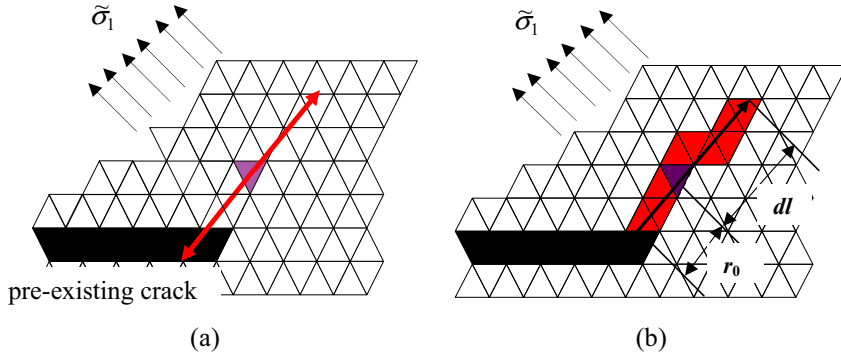


Fig. 3. Creation of the new crack. (a) Position and possible directions of the crack path. (b) Crack growth vector and element elimination.

6. In the crack growth direction, draw a line of length dl from \mathbf{x}_d . In the opposite direction, draw a line of length r_0 . Remove the elements through which these lines pass, as shown in Fig. 3b.
7. Resolve the linear elastic problem with the new structure. Calculate the total potential energy, noticed Π_2 ; Check the convergence $|dl + r_0 + \Delta\Pi/G_c| < \varepsilon$, where $\Delta\Pi = \Pi_2 - \Pi_1$ and ε is a preset tolerance value. Go to step 1 if convergence is attained.
8. Otherwise set $dl = \beta dl + (1 - \beta)(-\Delta\Pi/G_c - r_0)$, $0 < \beta < 1$.
9. If $dl \geq dl_0$, where dl_0 is a preset value, set $dl = dl_0$, go to 3.
10. Otherwise restore the removed elements at step 6 then go to step 6.

4. Validation of the non-local fracture criterion

As mentioned-above, the proposed non-local criterion is equivalent to the maximal principal stress criterion in the case of uniform tensile loading and to the Griffith–Irwin criterion in the case of a mode-I crack. The validation for the first case is trivial and does not need more comments. We focus our attention on the case of mode-I loaded cracks.

Consider a 2D square plate in PMMA (polymethylmethacrylate) with a central crack. The dimension of the specimen is $2W \times 2W = 10 \times 10 \text{ mm}^2$ with a central crack of different sizes, namely $a/W = 0, 0.02, 0.06, 0.1, 0.2, 0.4$ and 0.5 , here $a = 0$ represents a non-cracked plate. The mechanical properties of the material are: Young’s modulus $E = 3000 \text{ MPa}$, Poisson’s ratio $\nu = 0.3$, the ultimate stress $\sigma_c = 72 \text{ MPa}$, the critical stress intensity factor $K_{Ic} = 36 \text{ MPa} \sqrt{\text{mm}}$. With these material parameters and by using the analysis in Section 2, we can calculate the non-local action radius $R = 0.0835 \text{ mm}$ and the distance between the crack tip and the position of the maximal non-local principal stress $r_0 = 0.033 \text{ mm}$.

The plate was meshed with three-node triangle plane stress elements. In order to investigate the influence of meshing, different sizes of the elements near the crack tip are used in the simulations, namely $d = R/4, R/3, R/2$ and R , where d is the side length of the triangle elements. A pure tension along the normal direction of the crack was applied on the ends of the plate. By calculating the non-local first principal stresses and then finding their maximal value, we can easily determine the remote tensile stress at fracture according to the non-local fracture criterion (5). Then the stress intensity factor of such a central crack can be found from any handbook of stress intensity factors [46]. We compare the stress intensity factors thus obtained to the critical value K_{Ic} , and we can evaluate the accuracy of the method. The results of these calculations are shown in Fig. 4. In this

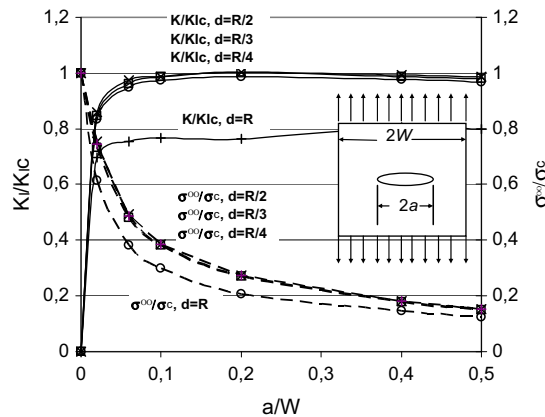


Fig. 4. Normalized stress intensity factor K_I/K_{Ic} and normalized remote stresses σ^∞/σ_c as function of normalized semi-crack length a/W for mode-I loaded cracks at fracture.

figure, the stress intensity factors are normalized by the critical value K_{Ic} ; the remote stresses at fracture are normalized by the ultimate stress σ_c of the material and the semi-crack length a is normalized by the semi-plate width W .

From this figure, we can observe that for sufficiently long cracks ($a/W > 0.05$), the normalized stress intensity factor $K_I/K_{Ic} \cong 1$. Therefore, the stress intensity factors at fracture evaluated by using the present non-local fracture criterion equal correctly the critical stress intensity factor of the material. Thus we demonstrate the equivalence between the proposed fracture criterion and the Griffith–Irwin criterion $K_I \geq K_{Ic}$. For short cracks, the present fracture criterion is no longer equivalent to the Griffith criterion that is not suitable to predict the short crack growth. The critical stress intensity factor decreases as the crack length decreases. Moreover, the remote stress at fracture tends to the material tensile strength as the crack length tends to zero. In this case, the proposed fracture criterion degenerates to the maximum principal stress criterion for non-singular stresses.

The mesh-independency of the crack prediction can be obtained by using sufficiently refined meshes. Apart from the results calculated with $d = R$ that represents quite a coarse meshing, the calculations with finer meshes, e.g. $d = R/4$, $R/3$ and $R/2$, provide us with nearly identical remote loads at fracture. In fact, the non-local action zone should contain enough number of elements in order to guarantee a good accuracy on the calculation of non-local stresses. The element size $d = R/2$ offers already sufficient accuracy for the crack growth prediction;

5. Thermal shock problem

In this section, we describe the application of the proposed non-local criterion in evaluating the cracking process in ceramic specimens under thermal shock.

Ceramic materials are widely used in various industries due to their excellent high temperature mechanical properties, corrosion resistance, wear resistance, erosion resistance, oxidation resistance, etc. However, their inherent brittleness and insignificant ductility make them particularly vulnerable to thermal shock failure. In general, crack formation is considered as the major reason of failure in thermo-structural engineering. Understanding the mechanisms of cracking process in ceramics under thermal loads has been one of the most important tasks in the research of this field.

Researches on fracture of ceramic materials underwent thermal shock was initiated 60 years ago by Kingery [47]. He first proposed a so called “critical stress” fracture criterion according to which cracks appear when the maximal thermal stress reaches the ultimate stress of the material. Hasselman [48] proposed a different approach in which the driving force for crack propagation is derived from the elastic energy stored in the body. In fact, these two different theories describe two different step of the fracture procedure during a thermal shock, i.e., the initiation and growth of macro-cracks. The non-local fracture model proposed in this work combines these theories in a single numerical framework that permits us to be able to predict both the initiation and growth of cracks in ceramics under thermal shock. Therefore, we can also say that the proposed method is congruent with the theories of Kingery and Hasselman and suitable to deal with fracture of ceramics subjected to thermal shock.

Ceramic materials undergo fast failure process under thermal shock, which leads to complex crack patterns. The multiple crack aspect in failure process renders the fracture assessment very difficult. Numerical difficulties can arise in simulating thermal shock induced fracture by using conventional fracture and damage models. For this reason, few numerical works have been reported in the literature so far due to the inherent complexities in multi-cracking modeling. Jiang et al. [49] carried out experimental and numerical works in determining the crack patterns by taking the temperature-dependence of the material parameters into account. On the basis of a variational approach, Bourdin et al. [50] developed a variational model capable to perform complicated fracture analysis in brittle materials under thermal shock.

In this paper, we present the numerical results obtained by using the present non-local fracture criterion and compare them with the experimental results.

5.1. Experiments

The experiments that we try to reproduce are those carried out by Jiang et al. [49]. In Jiang et al., 99% Al_2O_3 powder was thermoformed into 50 mm × 10 mm × 1 mm thin specimens. The specimens were tightly tied together with metallic wires in sets of five, with two additional thick ceramic plates on the outside to prevent the temperature distribution from being disturbed by coolant accessing the interior surfaces of the specimens. Then they were heated to a temperature T_0 ranged from 300 °C to 600 °C. After that, the heated specimens were dropped into a water bath of $T_\infty = 20$ °C by free fall. The crack pattern presents some typical characteristics. First, due to the small thickness of the specimens and the well-chosen temperature range, true two-dimensional crack patterns are observed. Second, a great number of cracks appear and form a complicated, periodic and hierarchical crack pattern. Third, the number of cracks increases whereas the crack spacing decreases as the initial temperature increases. We also observe a tendency towards equal spacing between cracks.

According to Kingery [47], multiple cracks appear when the thermal tensile stress due to surface shrinkage attains a critical level. These cracks will first grow simultaneously until the strain energy cannot support the simultaneous propagation of all cracks. At this moment, some cracks stop to propagate, whereas the others keep growing [51]. This process can repeat several times and then form a periodic and hierarchical crack pattern as observed in experiments.

In the following, we will attempt to reproduce these properties of crack patterns by direct numerical simulations.

5.2. Temperature field

The temperature field during the quenching test is the source of the stress concentration in the specimens and therefore must be firstly evaluated. The experimental conditions allow us to regard the temperature field as two-dimensional. Analytical solution exists for the thermal conduction of this kind of specimens. Establish a Cartesian coordinate system Oxy with the origin at the center of the specimen and x and y coinciding with the specimen axes. The transient temperature field $T = T(x, y, t)$ at any instant t in the specimen can be expressed as follows:

$$\frac{T - T_{\infty}}{T_0 - T_{\infty}} = \left[\sum_{m=1}^{\infty} X_m \exp\left(-\alpha_m^2 \frac{at}{L_1^2}\right) \cos\left(\alpha_m \frac{x}{L_1}\right) \right] \left[\sum_{m=1}^{\infty} Y_m \exp\left(-\beta_m^2 \frac{at}{L_2^2}\right) \cos\left(\beta_m \frac{y}{L_2}\right) \right] \quad (16)$$

where

$$X_m = \frac{2 \sin \alpha_m}{\alpha_m + \sin \alpha_m \cos \alpha_m}$$

$$Y_m = \frac{2 \sin \beta_m}{\beta_m + \sin \beta_m \cos \beta_m}$$

with α_m and β_m are the roots of the following transcendent equations:

$$\tan \alpha_m = \frac{hL_1}{k\alpha_m}$$

$$\tan \beta_m = \frac{hL_2}{k\beta_m} \quad (17)$$

where L_1 and L_2 are respectively the semi-length and semi-width of the specimen; h is the convective heat transfer coefficient; $a = k/\rho c$; k , ρ , c are the thermal conductivity, density and specific heat, respectively.

After numerical solution of (17), the temperature field can directly be obtained from (16). We assume that the cracking process does not influence the temperature field. This assumption is approximately justified by the fact that the cracks are essentially oriented in the temperature gradient direction.

5.3. Finite element model and material parameters

The ceramic specimens were assumed to be linearly elastic, homogeneous and isotropic. Fukuhura and Yamauchi [52] experimentally studied the temperature dependence of the Young's modulus and the Poisson ratio for alumina and reported that they remain approximately unchanged in the range 200–600 °C. An experimental report by De Smet and Bach [53] showed that the fracture toughness K_{IC} of two types of alumina differ slightly at 200 and 600 °C. Therefore, the mechanical characteristics are assumed to be constant and not influenced by temperature variation. From available data, Young's modulus E , Poisson's ratio ν , the ultimate tensile stress σ_c , the density ρ , and the energy release rate G of 99% Al_2O_3 ceramics are listed in Table 2 [54,55]. The critical stress intensity factor is deduced from $K_{IC} = \sqrt{GE}$. The non-local action radius deduced from (11) is $R = 0.063$ mm, $r_0 = 0.025$ mm.

Conversely, the thermal parameters such like the thermal conductivity k , the specific heat c and the thermal expansion coefficient α are temperature-dependent [56,57]. Consequently, adopting constant values in the quenching simulations is an approximate and simplified assumption. The values used in the simulations are listed in Table 2.

The thermal parameter that has a key influence on cracking process during the quenching tests is the convective heat transfer coefficient h . The available data give scattering estimations of this parameter and the mutual deviation is high up to an order of magnitude ($h \approx 10^4 \sim 10^5$ W/(m² K)) [56–60]. It is a common knowledge that this parameter depends on numerous factors such as the temperature of the bath and specimen temperature [58–62]. In this work, the so-called semi-inverse method described in Jiang et al. [49] is used to estimate the values of h at different temperature. This approach consists in finding an appropriate value of h for a temperature T_0 such that the calculated average crack spacing at the specimen surface agrees with that observed in experiments then the crack length, their periodical and hierarchical characteristics and their evolution are numerically predicted by using the proposed model with this h value. The values of h for different temperatures T_0 obtained by using this approach are listed in Table 3. For comparison, the h values estimated in Jiang et al. [49] by using the same approach are also listed in the table. Comparing these results, we remark that the same variation tendency is obtained in these two works, whereas in the present work, the variation of h is less pronounced than that obtained in Jiang et al. [49]. The differences between the values obtained in these two studies are essentially due to different assumptions adopted in these two works. We will return to this point in the next section.

The proposed non-local fracture model is an instantaneous damage model. An element is linearly elastic before its complete failure. Therefore, only linear elasticity solution is required in finite element modeling. This aspect of the approach

Table 2
Mechanical and thermal parameters used in the simulations.

E (MPa)	ν	σ_c (MPa)	P (kg/m ³)
370,000	0.3	220	3980
G (J/m ²)	k (W/(m K))	c (J/(kg K))	α
24.3	31	880	7.5×10^{-6}

Table 3
Heat transfer coefficient h (W/(m² K)) for different temperature T_0 .

T_0	300 °C	350 °C	400 °C	500 °C	600 °C
Present work	65,000	90,000	82,000	70,000	60,000
Jiang et al. [49]	54,500	100,000	86,000	57,000	45,000

avoids the costly and complicated algorithm for non-linear solution. However, iterations are needed for the determination of the crack growth length dl according to (15). Nevertheless, no extraordinary accuracy is required in this calculation since the real increment of dl is necessarily times of the element size when we use the element elimination technique. The convergence tolerance on dl that we used is about the tenth of the element size.

By taking the symmetry of the specimen into account, only a quarter of it was meshed by finite elements. The specimen was meshed with three-node plane stress elements. The side size of the elements is about $d = 0.021$ mm, e.g. about a third of the non-local action radius R . The 2D finite element discretization of the specimen contains about 570,000 elements and 650,000 degrees of freedom. This is quite a refined discretization comparing with respect to the specimen size (25×5 mm²). As the damage bands have a width of one element size, the damaged bands are very narrow and can be considered as sharp cracks. Using coarser discretization $d = R/2$ provided very similar numerical results. Based on our experience, the time interval in the simulation was set from 10^{-5} to 1 s. The time increment is 10^{-5} s at the beginning and gradually increases to about 0.05 s at the end of the simulation.

6. Numerical results and discussions

6.1. Crack initiation at the specimen surface

As we have analysed, the crack initiation and growth depend uniquely on the level of the non-local first principal stresses. Let us examine the distribution of the non-local first principal stress just before the crack initiation in the specimens. Fig. 9 shows its distributions along the longer edge of the specimen.

In an earlier analysis [49], this type of specimens is considered as infinitely long with perfect uniformly distributed stress along the specimen edge. Consequently, the crack initiation is considered as instantaneous and simultaneous. However, even though the material is considered as perfectly homogeneous in the simulation, the stress distribution is not perfectly uniform for specimens with finite size. Fig. 5 shows the maximal principal stress distribution along the longer edge of the specimen. We observe clearly a maximal stress value at a point on the edge where the first crack should initiate before others. Therefore, the crack initiations are not exactly simultaneous but successive one after another. From this point of view, the successive crack initiation predicted by present method is physically more reasonable.

In Fig. 6, we show the positions of the first crack onsets and the non-local first principal stress distribution in the specimen at this instant. When the non-local criterion is fulfilled at a point, a crack is created according to the proposed criterion and the described algorithm. As a consequence, the stress relaxation takes place at the vicinity of this point. Then the algorithm will find another position where the non-local principal stress is maximal and create a crack if the fracture criterion is fulfilled. This procedure will repeat until the temperature gradient is no longer capable to produce sufficient stress concentration to onset new cracks. Then a time increment will provide a new temperature map that may probably lead to new cracking process.

In Fig. 7, the crack patterns obtained with numerical simulations are illustrated for different instants during the quenching test. The different colors indicate the levels of the maximal principal stress such that the stress concentrations can be distinguished. The removed elements are colored in black, and then the crack formation by removing successively

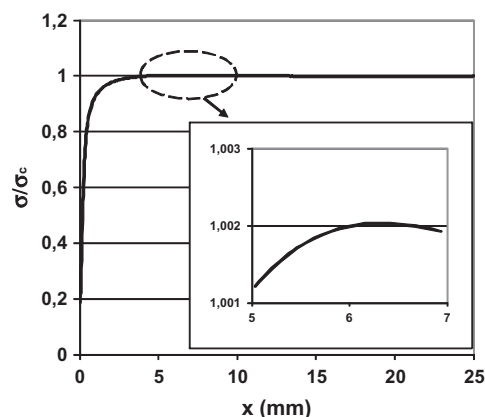


Fig. 5. Distribution of the non-local first principal stress along the specimen edge.

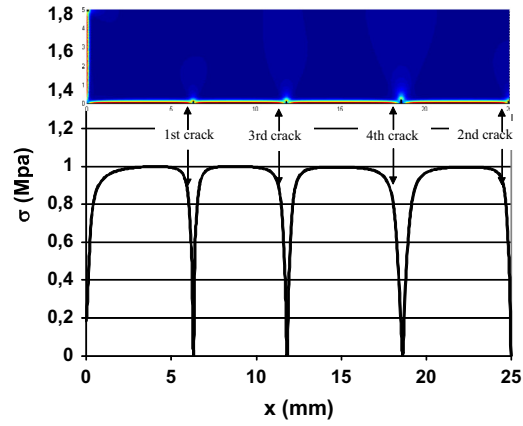


Fig. 6. First crack onsets and stress redistribution on the specimen border.

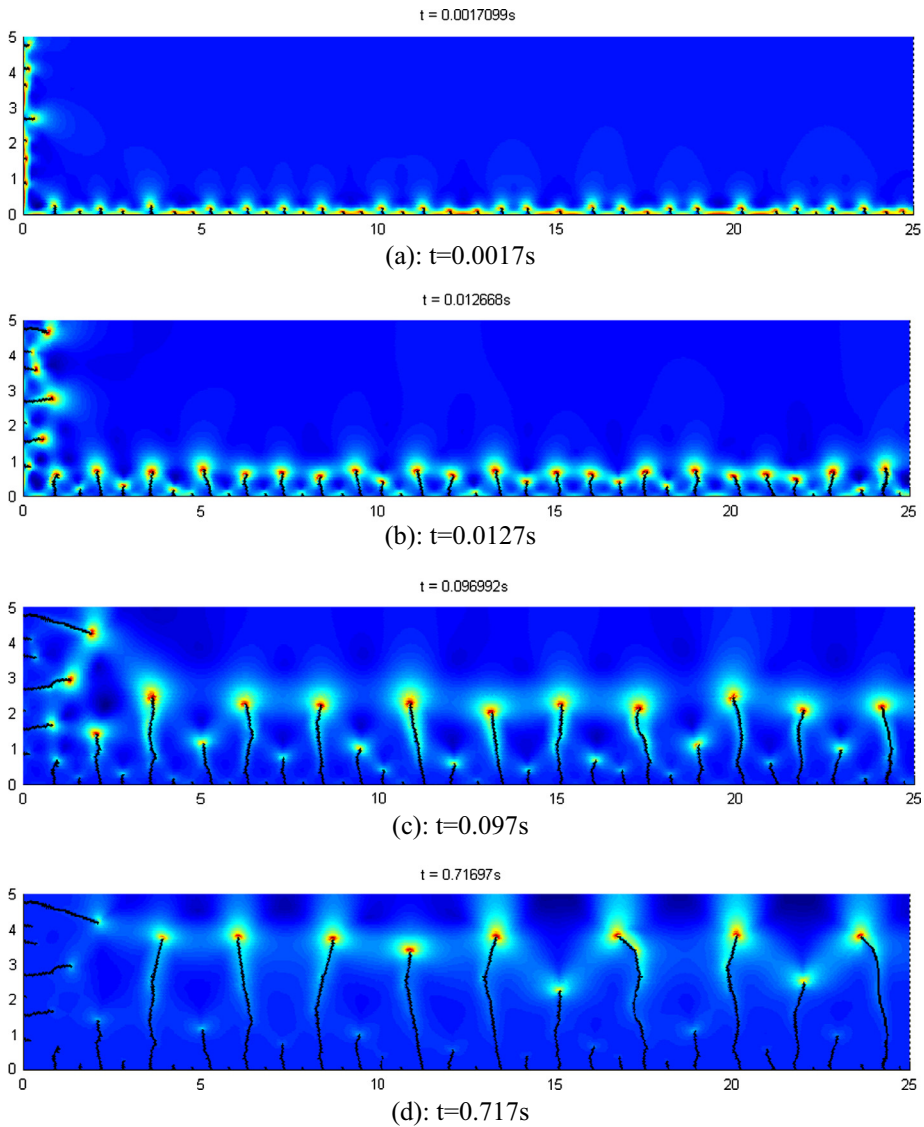


Fig. 7. Simulation results on crack patterns at different times after quenching, $T_0 = 500\text{ }^\circ\text{C}$.

the damaged elements can clearly be observed. These images confirm the scenario of the cracking process during the quenching described in earlier works [49]. At the beginning, the thermal shock cracks initiate at a critical time (about 10^{-3} s after the quenching). All cracks appear within a very short time with a nearly equal spacing, then they propagate uniformly and rapidly (Fig. 7a). Then the propagation speed decreases gradually until some of them stop growing. Only a reduced number of cracks continue to propagate such that the crack spacing increases until 2 or 3 times larger (Fig. 7b). In the following, the crack growth may deviate and attempt to form equal crack spacing (Fig. 7c). The final simulation crack patterns (Fig. 7d) are very similar to those observed in experimental results. This remark supports the cracking process above described.

6.2. Direct comparison with the experiments

Fig. 8 illustrates the final crack patterns of the numerical simulations for different initial quenching temperatures. Even though the random effects such as the ceramic micro-structural heterogeneity and the experimental non-deterministic factors have not been taken into account in the numerical simulations, we can confirm that the simulations of the present work reproduce faithfully the crack patterns obtained from quenching tests.

Globally speaking, the simulation results shown in Fig. 8 reproduce all the essential characteristics of the real crack patterns: Multiple cracks are obtained for different initial quenching temperatures; The cracks initiate on the contour and

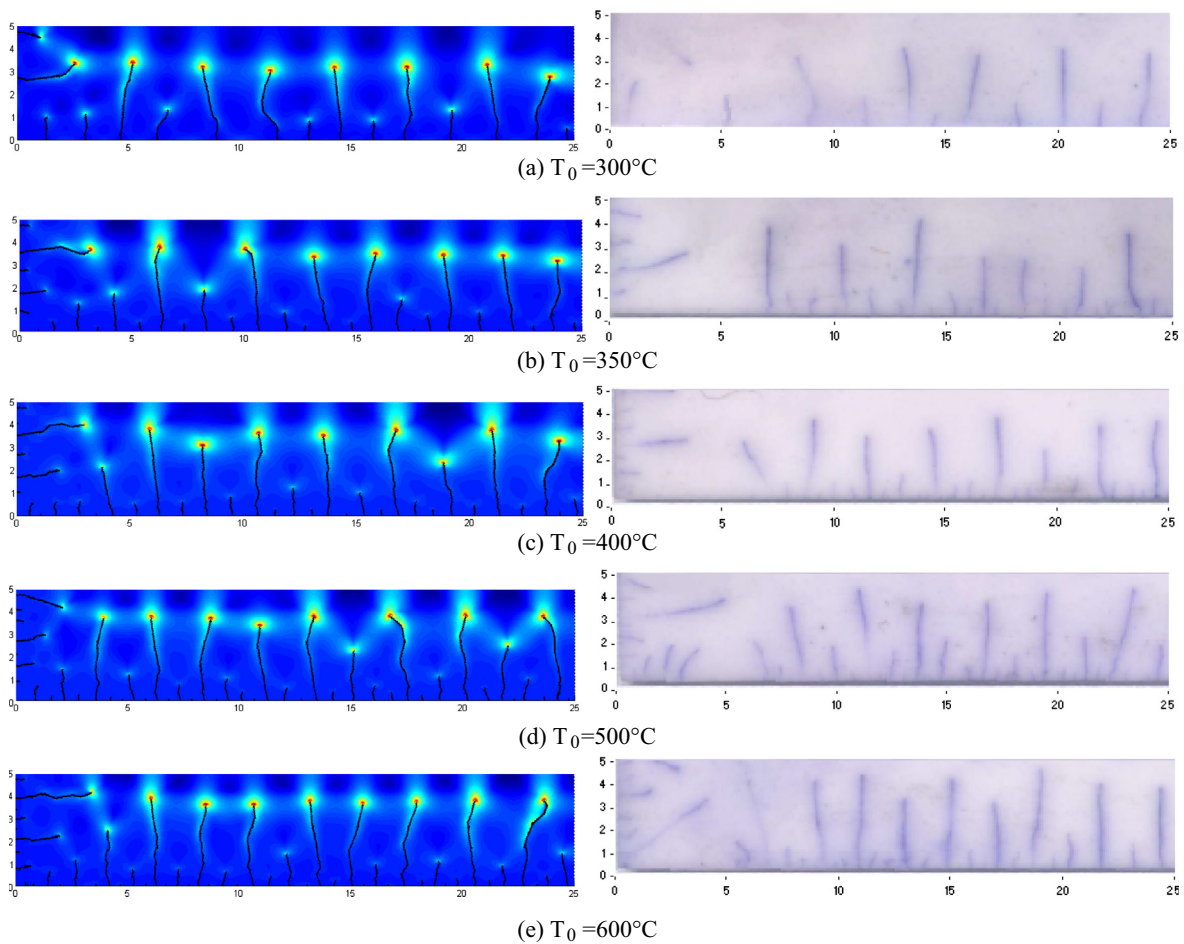


Fig. 8. Comparison between the crack patterns in numerical models and in real specimens.

Table 4

Dimensionless crack length $\bar{p} = p/L_2$.

	$T_0 = 300\text{ }^\circ\text{C}$	$T_0 = 350\text{ }^\circ\text{C}$	$T_0 = 400\text{ }^\circ\text{C}$	$T_0 = 500\text{ }^\circ\text{C}$	$T_0 = 600\text{ }^\circ\text{C}$
Numerical results	0.68	0.71	0.72	0.76	0.76
Test [49]	0.71	0.73	0.72	0.77	0.79

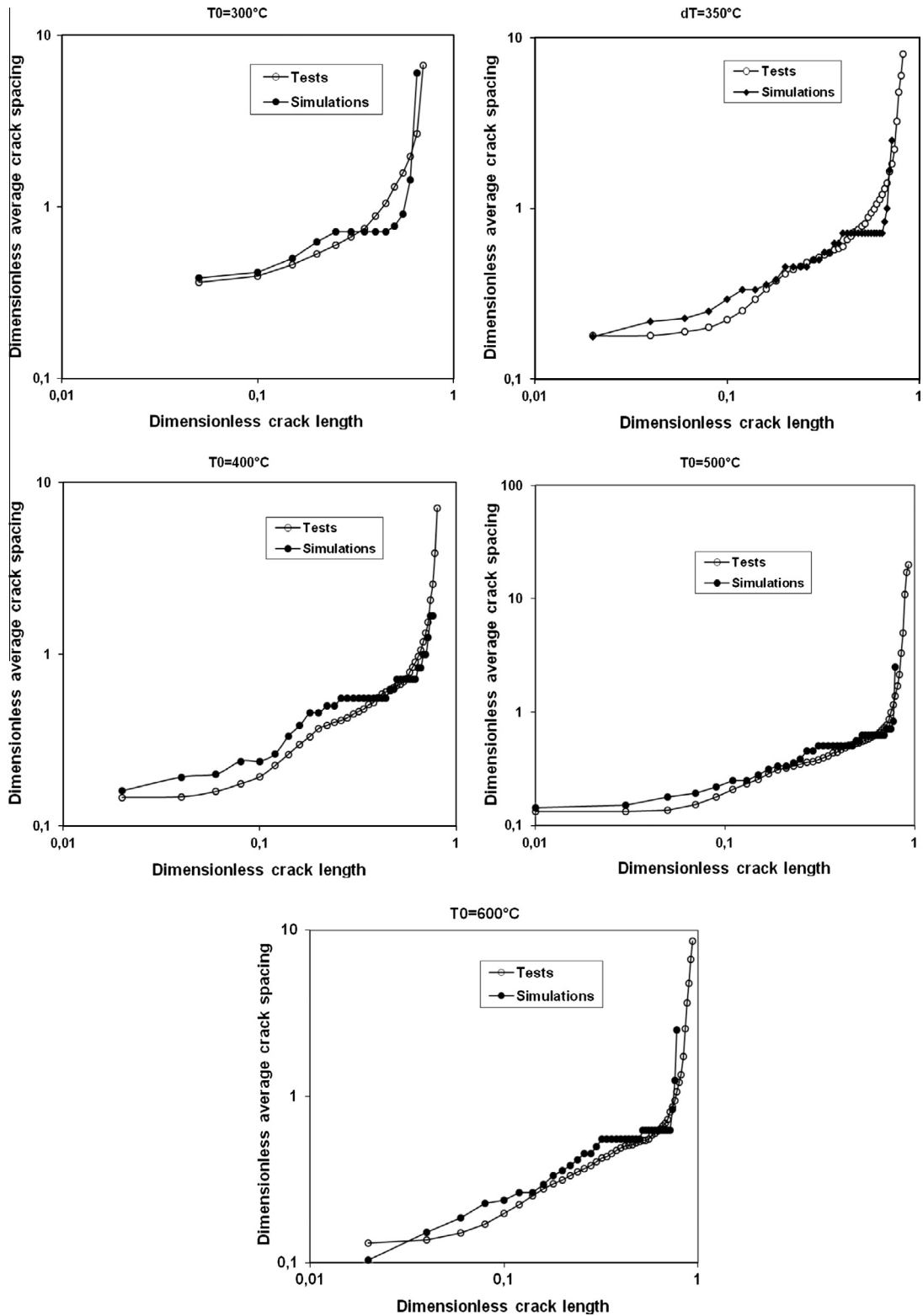


Fig. 9. Normalized crack spacing $\bar{s} = s/L_2$ vs normalized crack length $\bar{p} = p/L_2$.

propagate into the interior of the specimens; Periodical and hierarchical crack structure is correctly reproduced; We also observe a tendency towards equal spacing between cracks during all the cracking process as in real specimens.

6.3. Characteristic values of the crack patterns

In general, the numerical simulations provide more regular crack patterns comparing to those in real specimens. This is because that the material heterogeneities in the real material at microscopic level have not been included in the modeling. However, statistically speaking, the principal features of the crack patterns can be brought out from numerical results. In Table 4, we compare the average lengths of the long cracks in numerical and experimental crack patterns. The term “long crack” in the present work means that the dimensionless crack length $\bar{p} = p/L_2 \geq 0.6$, where p denotes the crack length. Generally speaking, very good agreement is obtained between all the numerical simulations and the experiments.

Another useful comparison is made in Fig. 9 on the diagram “crack spacing vs crack length”. According to Bahr et al. [63], this diagram can serve as justification for applying a model to a real material. Fig. 9 shows the comparison between the experimental and numerical results on such curves. In Fig. 9, the average crack spacing s has been determined by counting the intersection points of cracks with a straight line in the depth p . These values were normalized by the semi-width of the specimens to obtain the corresponding dimensionless values $\bar{s} = s/L_2$ and $\bar{p} = p/L_2$. The experimental results are obtained from statistics over 5 specimens while the numerical results are issued from one simulation for each initial quenching temperature. Because of the hierarchy feature of the cracks, the crack spacing decreases as the crack length increases. We can remark that this tendency is respected by both the experimental and numerical results. However, the experimental curves are smoother, indicating the less distinct hierarchy of crack lengths in real specimens, due to the randomness of initial flaws and non-determinist aspects in experiments. In contrast, the numerical results exhibit several jumps and plateaux, indicating a more pronounced hierarchical feature as the random factors are not considered in the numerical models. Apart from this point, it is shown that the numerical model and the experiments agree unexpectedly well.

7. Concluding remarks

In this work, a non-local failure model was proposed to predict crack initiation and crack growth in a 2D structure made of brittle materials. It was then implemented into a finite element code. This non-local fracture model was successfully applied to simulating the crack evolution in ceramic materials subjected to thermal shock. From the results of the numerical simulations, the following conclusions can be formulated:

1. The proposed non-local fracture model is equivalent to the maximum principal stress criterion for a specimen under pure tensile loading, and to the Griffith–Irwin criterion for the crack propagation. The other stress states can be considered as a natural interpolation between these two extreme situations. This aspect ensures a good accuracy in crack onset and crack growth predictions.
2. The implementation of the non-local fracture criterion into a finite-element code provides an efficient numerical tool for cracking process prediction. The numerical results on the prediction of the critical loads at fracture and crack paths are independent of meshing when the size of the element is sufficiently small.
3. The numerical simulation reproduced faithfully the multi-cracking process and the crack patterns in ceramic specimens subjected to quenching tests. The periodical and hierarchical characteristics of the crack patterns were accurately predicted. The parameters describing the crack patterns such as the average crack spacing and the crack lengths were correctly estimated from the numerical results. The numerical simulations allow a direct observation on crack initiation and growth in the specimens, which is quite a difficult task in experimental studies.

Acknowledgements

This work was supported by the funding from the French ANR program T-Shock ANR-10-INTB-0915 and the National Natural Science Foundations of China (Grants Nos. 11061130550 and 11172023).

References

- [1] Lemaitre J, Chaboche JL. *Mechanics of solid materials*. Cambridge: Cambridge University Press; 1990.
- [2] Lemaitre J. *A course on damage mechanics*. Berlin: Springer; 1992.
- [3] De Borst R. Computation of post-bifurcation and post-failure behaviour of strain-softening solid. *Comp Struct* 1987;25:211–24.
- [4] Bazant ZP, Lin FB. Nonlocal smeared crack model for concrete fracture. *J Engng Mech, ASCE* 1998;114:2493–510.
- [5] Maire JF, Chaboche JL. A new formulation of continuum damage mechanics (CDM) for composite materials. *Aerosp Sci Technol* 1997;1:247–57.
- [6] Bhattacharya B, Ellingwood B. Continuum damage mechanics analysis of fatigue crack initiation. *Int J Fatigue* 1998;20:631–9.
- [7] Barenblatt G. The formation of equilibrium cracks during brittle fracture. *J Appl Math Mech* 1959;23:434–44.
- [8] Dugdale D. Yielding of steel sheets containing slits. *J Mech Phys Solids* 1960;8:100–4.
- [9] Xu XP, Needleman A. Numerical simulation of fast crack growth in brittle solids. *J Mech Phys Solids* 1994;42:1397–434.
- [10] Camacho GT, Ortiz M. Computational modelling of impact damage in brittle materials. *Int J Solids Struct* 1996;33:2899–938.
- [11] Mohammed I, Liechti KM. Cohesive zone modelling of crack nucleation at bimaterial corners. *J Mech Phys Solids* 2000;48:735–64.

- [12] Belytschko T, Black T. Elastic crack growth in finite elements with minimal remeshing. *Int J Numer Meth Engng* 1996;45:601–20.
- [13] Moës N, Dolbow J, Belytschko T. A finite element method for crack growth without remeshing. *Int J Numer Meth Engng* 1999;46:131–50.
- [14] Dolbow J, Moës N, Belytschko T. Discontinuous enrichment in finite element with a partition of unity method. *Finite Elem Anal Des* 2000;36:235–60.
- [15] Belytschko T, Moës N, Usui S, Parimi C. Arbitrary discontinuities in finite elements. *Int J Numer Meth Engng* 2001;50:993–1013.
- [16] Mariani S, Perego U. Extended finite element method for quasi brittle fracture. *Int J Numer Meth Engng* 2003;58:103–26.
- [17] Francfort G, Marigo JJ. Revisiting brittle fracture as an energy minimization problem. *J Mech Phys Solids* 1998;46:1319–42.
- [18] Bourdin B, Francfort G, Marigo JJ. Numerical experiments in revisited brittle fracture. *J Mech Phys Solids* 2000;48:797–826.
- [19] Bourdin B, Francfort G, Marigo JJ. The variational approach to fracture. *J Elast* 2008;91:5–148.
- [20] Pijaudier-Cabot G, Bazant ZP. Nonlocal damage theory. *J Engng Mech, ASCE* 1987;113:1512–33.
- [21] Pijaudier-Cabot G, Burlion N. Damage and localization in elastic materials with voids. *Mech Cohes-Frict Mater* 1996;1:129–44.
- [22] Peerlings R, Geers M, de Borst R, Brekelmans W. A critical comparison of non-local and gradient-enhanced softening continua. *Int J Solids Struct* 2001;38:7723–46.
- [23] Frémond M, Nedjar B. Damage, gradient of damage and principle of virtual power. *Int J Solids Struct* 1996;33:1083–103.
- [24] Ostojia-Starzewski M, Sheng PY, Alzabdeh K. Spring network models in elasticity and fracture of composites and polycrystals. *Comput Mater Sci* 1996;7:82–93.
- [25] Lilliu G, van Mier JGM. 3D lattice type fracture model for concrete. *Engng Fract Mech* 2003;70:927–41.
- [26] Karihaloo BL, Shao PF, Xiao QZ. Lattice modelling of the failure of particle composites. *Engng Fract Mech* 2003;70:2385–406.
- [27] Carpinteri A, Ciola F, Pugno N. Boundary element method for the strain-softening response of quasi-brittle materials in compression. *Comput Struct* 2001;79:389–401.
- [28] Carpinteri A, Yang GP. Size effects in brittle specimen with micro crack interaction. *Comput Struct* 1997;63:429–37.
- [29] Zhang XB, Li J, Boukha SE. Modelling the failure behaviour of brittle or quasi-brittle materials by analyzing the growth of micro-cracks. *Int J Fract* 2009;160:73–83.
- [30] Neuber H. *Kerbspannungslehre*. Berlin: Springer; 1937.
- [31] Novozhilov VV. On necessary and sufficient criterion of brittle strength. *Appl Math Mech (PMM)* 1969;33:212–22.
- [32] Seweryn A. Brittle fracture criterion for structures with sharp notches. *Engng Fract Mech* 1994;47(4):673–81.
- [33] Pluvinage G. *Fracture and fatigue emanating from stress concentrators*. Dordrecht: Kluwer; 2003.
- [34] McClintock FA. Ductile fracture instability in shear. *J Appl Mech* 1958;10:582–8.
- [35] Linear Irwin G. Linear fracture mechanics, fracture transition and fracture control. *Engng Fract Mech* 1968;1:241–57.
- [36] Cheng CZ, Recho N, Niu ZR. Influence of the non-singular stress on the crack extension and fatigue life. *Nucl Engng Des* 2012;248:293–300.
- [37] Li J. A strain gradient model for fracture prediction in brittle materials. *J Appl Mech, ASME* 2008;75:1–9.
- [38] Leguillon D. Strength or toughness? A criterion for crack onset at a notch. *Euro J Mech A/Solids* 2002;21:61–72.
- [39] Li J, Pham T, Abdelmoula R, Song F, Jiang CP. A micromechanics-based strain gradient damage model for fracture prediction of brittle materials – part II: damage modeling and numerical simulations. *Int J Solids Struct* 2011;48:3346–58.
- [40] Li J, Tian XX, Abdelmoula R. A damage model for crack prediction in brittle and quasi-brittle materials solved by the FFT method. *Int J Fract* 2012;173:135–46.
- [41] Li J, Meng SH, Tian XX, Song F, Jiang CP. A non-local fracture model for composite laminates and numerical simulations by the FFT method. *Composites B* 2012;43:961–71.
- [42] Griffith A. The phenomena of rupture and flow in solids. *Philos Trans Royal Soc* 1920;221:163–98.
- [43] Irwin G. Linear fracture mechanics, fracture transition and fracture control. *Engng Fract Mech* 1968;1:241–57.
- [44] Williams ML. Stress singularities resulting from various boundary conditions in angular corners of plates in extension. *ASME J Appl Mech* 1952;19:526–8.
- [45] Jiang DL, Li LT, Ouyang SHX, Shi JL. *China materials engineering canon*. Beijing: Chemical Industry Press; 2006 [in Chinese].
- [46] Sih G. *Handbook of stress-intensity factors*. Lehigh University; 1973.
- [47] Kingery WD. Factors affecting thermal stress resistance of ceramic materials. *J Am Ceram Soc* 1955;38:3–15.
- [48] Hasselman DPH. Approximate theory of thermal stress resistance of brittle ceramics involving creep. *J Am Ceram Soc* 1969;50:454–7.
- [49] Jiang CP, Wu XF, Li J, Song F, Shao YF, Xu XH, et al. A study of the mechanism of formation and numerical simulations of crack patterns in ceramics subjected to thermal shock. *Acta Mater* 2012;60:4540–50.
- [50] Bourdin B, Maurini C. *A variational approach to thermal fracture, XXIII ICTAM*. Beijing; 2012. p. 19–24.
- [51] Jenkins DR. Optimal spacing and penetration of cracks in a shrinking slab. *Phys Rev E* 2005;71(5):056117.
- [52] Fukuhara M, Yamauchi I. Temperature-dependence of the elastic-moduli, dilatational and shear internal frictions and acoustic-wave velocity for alumina, (Y)TZP and β -sialon ceramics. *J Mater Sci* 1993;28:4681–8.
- [53] De Smet BJ, Bach PW. High temperature fracture toughness of alumina, ferrite and silicon carbide. The Nether-lands Energy Research Foundation, ECN-C-92-083; 1992.
- [54] Zhang YL, Ma JP. *Applicable ceramic material manual*. Beijing: Chemical Industry Press; 2006 [in Chinese].
- [55] Zhang QY. *Mechanical properties of ceramics*. Beijing: Science Press; 1987 [in Chinese].
- [56] Touloukian YS, Ho CY. *Thermophysical properties of matter, thermal conductivity of nonmetallic solids, vol. 2*. New York: Plenum Press; 1972.
- [57] Touloukian YS, Ho CY. *Thermophysical properties of matter, specific heat of nonmetallic solids, vol. 5*. New York: Plenum Press; 1972.
- [58] Singh JP, Tree Y, Hasselman DPH. Effect of bath and specimen temperature on the thermal stress resistance of brittle ceramics subjected to thermal quenching. *J Mater Sci* 1981;16:2109–18.
- [59] Becher PF. Effect of water bath temperature on the thermal shock of Al_2O_3 . *J Am Ceram Soc* 1981;64:C17–8.
- [60] Kim Y, Lee WJ, Case ED. The measurement of the surface heat transfer coefficient for ceramics quenched into a water bath. *Mater Sci Engng, A* 1991;145:L7–C11.
- [61] Lee WJ, Kim Y, Case ED. The effect of quenching media on the heat transfer coefficient of polycrystalline alumina. *J Mater Sci* 1993;28:2079–83.
- [62] Zhou ZL, Song F, Shao YF, Meng SH, Jiang CP, Li J. Characteristics of the surface heat transfer coefficient for Al_2O_3 ceramic in water quench. *J Euro Ceram Soc* 2012;32:3029–34.
- [63] Bahr HA, Weiss HJ, Maschke HG, Meissner F. Multiple crack propagation in a strip caused by thermal shock. *J Mech Phys Solids* 2010;58:1411–21.